radius of 1350 ± 5 km (T. Johnson, personal communication) and a 1-s (~20-km) uncertainty in the spacecraft trajectory. At the lowest atmospheric levels probed by the occultation, the signals do not go smoothly to zero but appear to cease abruptly, supporting our contention that the source has passed below the limb.
22. Because of the low temperatures, we expect that the abundance of other potential absorbers, such as C_2H_2, C_2H_6, and hydrogen cyanide (HCN), will be limited to negligible levels by their vapor pressures.
23. Use of this model for Triton was suggested to us by E. Lellouch. See E. Lellouch *et al.*, *Icarus*, in press.
24. B. A. Smith *et al.*, *Science* **246**, 1422 (1989).
25. G. L. Tyler *et al.*, *ibid.*, p. 1466.
26. R. B. Leighton and B. C. Murray, *Science* **153**, 136 (1966).
27. L. M. Trafton, *Icarus* **58**, 293 (1984).
28. The mixing ratio is $f = QH/b$, where Q is the production rate, equal to the upward flux, H is the scale height at the homopause (20 km), and $b = 3.5 \times 10^{18}$ cm^{-1} s^{-1} is the product of diffusion coefficient and number density [D. M. Hunten, *J. Atmos. Sci.* **30**, 726 (1973)].
29. A. L. Lane *et al.*, *Science* **246**, 1450 (1989).
30. N. F. Ness *et al.*, *ibid.*, p. 1473.
31. We thank M. Summers for performing photochemical calculations and M. Stevens for thermal conduction calculations in support of this analysis. We thank J. Stansberry for aerosol production calculations and V. Eshleman for helpful discussions. We thank the Voyager Project personnel at the Jet Propulsion Laboratory for their enthusiastic efforts that have made this mission successful. We acknowledge the work of the Voyager Spacecraft Team, particularly G. Hanover and H. Marderness, whose fine tuning of scan platform pointing and spacecraft stabilization led to exceptionally good occultation observations during this encounter. Supported by the Jet Propulsion Laboratory, California Institute of Technology, under National Aeronautics and Space Administration (NASA) contract NAS1-100. Additional support was provided by the Planetary Sciences Discipline of NASA's Office of Space Sciences.

31 October 1989; accepted 15 November 1989

Voyager Radio Science Observations of Neptune and Triton

G. L. TYLER, D. N. SWEETNAM, J. D. ANDERSON, S. E. BORUTZKI, J. K. CAMPBELL, V. R. ESHLEMAN, D. L. GRESH, E. M. GURROLA, D. P. HINSON, N. KAWASHIMA, E. R. KURSINSKI, G. S. LEVY, G. F. LINDAL, J. R. LYONS, E. A. MAROUF, P. A. ROSEN, R. A. SIMPSON, G. E. WOOD

The Voyager 2 encounter with the Neptune system included radio science investigations of the masses and densities of Neptune and Triton, the low-order gravitational harmonics of Neptune, the vertical structures of the atmospheres and ionospheres of Neptune and Triton, the composition of the atmosphere of Neptune, and characteristics of ring material. Demanding experimental requirements were met successfully, and study of the large store of collected data has begun. The initial search of the data revealed no detectable effects of ring material with optical depth $\tau \lesssim 0.01$. Preliminary representative results include the following: 1.0243×10^{26} and 2.141×10^{22} kilograms for the masses of Neptune and Triton; 1640 and 2054 kilograms per cubic meter for their respective densities; 1355 ± 7 kilometers, provisionally, for the radius of Triton; and $J_2 = 3411 \pm 10(\times10^{-6})$ and $J_4 = -26^{+12}_{-20}(\times10^{-6})$ for Neptune's gravity field (J_2 and J_4 are harmonic coefficients of the gravity field). The equatorial and polar radii of Neptune are 24,764 ± 20 and 24,340 ± 30 kilometers, respectively, at the 10^5-pascal (1 bar) pressure level. Neptune's atmosphere was probed to a pressure level of about 5×10^5 pascals, and effects of a methane cloud region and probable ammonia absorption below the cloud are evident in the data. Results for the mixing ratios of helium and ammonia are still being investigated; the methane abundance below the clouds is at least 1 percent by volume. Derived temperature-pressure profiles to 1.2×10^5 pascals and 78 kelvins (K) show a lapse rate corresponding to "frozen" equilibrium of the para- and ortho-hydrogen states. Neptune's ionosphere exhibits an extended topside at a temperature of 950 ± 160 K if H^+ is the dominant ion, and narrow ionization layers of the type previously seen at the other three giant planets. Triton has a dense ionosphere with a peak electron concentration of 46×10^9 per cubic meter at an altitude of 340 kilometers measured during occultation egress. Its topside plasma temperature is about 80 ± 16 K if N_2^+ is the principal ion. The tenuous neutral atmosphere of Triton produced distinct signatures in the occultation data; however, the accuracy of the measurements is limited by uncertainties in the frequency of the spacecraft reference oscillator. Preliminary values for the surface pressure of 1.6 ± 0.3 pascals and an equivalent isothermal temperature of 48 ± 5 K are suggested, on the assumption that molecular nitrogen dominates the atmosphere. The radio data may be showing the effects of a thermal inversion near the surface; this and other evidence imply that the Triton atmosphere is controlled by vapor-pressure equilibrium with surface ices, at a temperature of 38 K and a methane mixing ratio of about 10^{-4}.

VOYAGER RADIO SCIENCE (RSS) observations of the Neptune system comprise coherent radio Doppler and ranging measurements for the study of Neptune's gravity and the mass of Triton, radio occultation measurements of the atmosphere of Neptune and Triton, and a radio occultation search for Neptune's ring arcs. Experimental and analytical techniques are similar to those used previously (*1, 2*), with the exception that for Triton the technique of diffraction correction developed for the study of planetary rings was extended for the first time to the study of atmospheres.

The occultation experiments are based on the geometry obtained as Voyager passed behind Neptune and Triton (Fig. 1). Unmodulated, dual-frequency transmissions at wavelengths of 3.6 and 13 cm from Voyager's telecommunication transmitters (*3*) were used to probe the intervening atmosphere and possible ring material. These signals were received simultaneously at three tracking stations: the 70-m (diameter) antenna of the National Aeronautics and Space Administration (NASA) Deep Space Network at Tidbinbilla, Australia, received both wavelengths, while the 64-m Commonwealth Scientific and Industrial Research Organization (CSIRO) antenna at Parkes, Australia, received only the 3.6-cm signal, and the 64-m Institute of Space and Astronautical Science antenna at Usuda, Japan, received only the 13-cm signal. Provisions were made for coherent arraying of the stations during future data reduction for the purpose of improving the signal-to-noise ratio (*4*).

We report here preliminary results for the gravity field of Neptune, the mass and density of Triton, the ionosphere and atmosphere of Neptune, and the ionosphere and atmosphere of Triton, including a measurement of the surface pressure of Triton. These initial results are based on a combination of data from the real-time tracking and monitoring systems used in collecting the data (*5*) and from a limited analysis of the primary data from the Tidbinbilla station (*6*). Nep-

G. L. Tyler, V. R. Eshleman, D. L. Gresh, E. M. Gurrola, D. P. Hinson, E. A. Marouf, P. A. Rosen, R. A. Simpson, Stanford University, Stanford, CA 94305.
D. N. Sweetnam, J. D. Anderson, S. E. Borutzki, J. K. Campbell, E. R. Kursinski, G. S. Levy, G. F. Lindal, J. R. Lyons, G. E. Wood, Jet Propulsion Laboratory, California Institute of Technology, Pasadena, CA 91109.
N. Kawashima, Institute of Space and Astronautical Science, Sagamihara, 229 Japan.

tune's rings were not detected in the data examined to this point at a sensitivity of $\sigma_\tau \approx 0.01$ and a radial resolution of 2 km; this limit does not apply to the ring "arcs," however, as these portions of the rings were not probed by our experiment (*7*).

Masses of Neptune and Triton. The total mass of the Neptune system (Neptune and its satellites) was determined from data collected about 35 hours before encounter by the Voyager navigation team, to an accuracy more than 100 times better than previously achieved (*8*). By combining pre-encounter navigation data with coherent Doppler data obtained for the RSS team during encounter, we gained about another factor of 10 improvement because of close approaches to Neptune and Triton during the flyby. We discuss masses in terms of both mass M in kilograms and GM in the commonly used units of $km^3\ s^{-2}$, using the gravitational constant $G = 6.6728 \times 10^{-11}\ m^3\ kg^{-1}\ s^{-2}$. Because measurement accuracies for GM can exceed the accuracy to which G is known, uncertainties are given only for GM.

The most fundamental result from the coherent Doppler data is for the Neptune system, where our preliminary analysis yields $GM_{sys} = 6{,}836{,}534 \pm 20\ km^3\ s^{-2}$ or $M_{sys} = 1.0245 \times 10^{26}$ kg. For purposes of celestial mechanics within the solar system, the derived ratio of the mass of the sun to the mass of the Neptune system is 19412.249 ± 0.057 (*9*). (Uncertainties here and throughout this report are $\pm 1\sigma$ error limits, unless noted.)

When a spacecraft flies through a planetary system consisting of a planet and one or more satellites, the trajectory deviations reveal, in principle, the masses of the individual bodies as well as the system mass. With the Voyager 2 flyby of Neptune, the masses of the planet and Triton were easily distinguishable. Even the small satellites Nereid and 1989N1 were detected, the former by the barycentric motion of Neptune and the latter by direct gravitational attraction, but it will take considerably more data analysis to determine if their masses can be specified to within an accuracy of 50%.

Our preliminary result for Triton is $GM_{Tr} = 1428.5 \pm 4.5\ km^3\ s^{-2}$ or $M_{Tr} = 2.141 \times 10^{22}$ kg. Using a radius of 1355 ± 7 km (*10*) and assuming a spherical shape, we derive a mean density of $2054 \pm 32\ kg\ m^{-3}$, where the error is due primarily to the uncertainty in the radius. In terms of the ice-rock ratio (*11*), Triton is clearly not a satellite in the class of Ganymede, Callisto, and Titan but instead is very similar to the planet Pluto.

For Neptune, we subtract the Triton mass from the system mass and subtract an additional $GM = 10\ km^3\ s^{-2}$ to account for the small satellites and rings. Thus $GM_{Nep} = 6{,}835{,}096 \pm 21\ km^3\ s^{-2}$, $M_{Nep} = 1.0243 \times 10^{26}$ kg, and the mean density is 1640 kg m^{-3}. Neptune has the highest mean density of the four giant planets. The values for Jupiter, Saturn, and Uranus are 1326, 686, and 1267 kg m^{-3}, respectively, where the 10^5-Pa (1 bar) atmospheric pressure level is used for defining size and shape (*12*).

Gravity field. Because of the close flyby of Neptune in a near polar trajectory, we are able to use the coherent Doppler data to investigate the zonal harmonics of Neptune's gravity field. We include both even and odd harmonic coefficients J_2 through J_6 in the data analysis, as well as the right ascension and declination of Neptune's north polar axis. All other harmonic coefficients are assumed exactly zero. The reference radius for all the harmonic coefficients is 25,225 km. One can determine the quadrupole moment J_2 by solving via least-squares analysis for the five zonal harmonics or by solving for only the even ones. In all our solutions we included important outside information on the pole location by obtaining a solution for the pole and its associated covariance matrix from ground-based data on the orbit of Triton (*13*). Our current best estimate of J_2 from a number of solutions, some of which include a priori information from the navigation targeting solutions and some of which do not, is 3411 ± 10 $(\times 10^{-6})$.

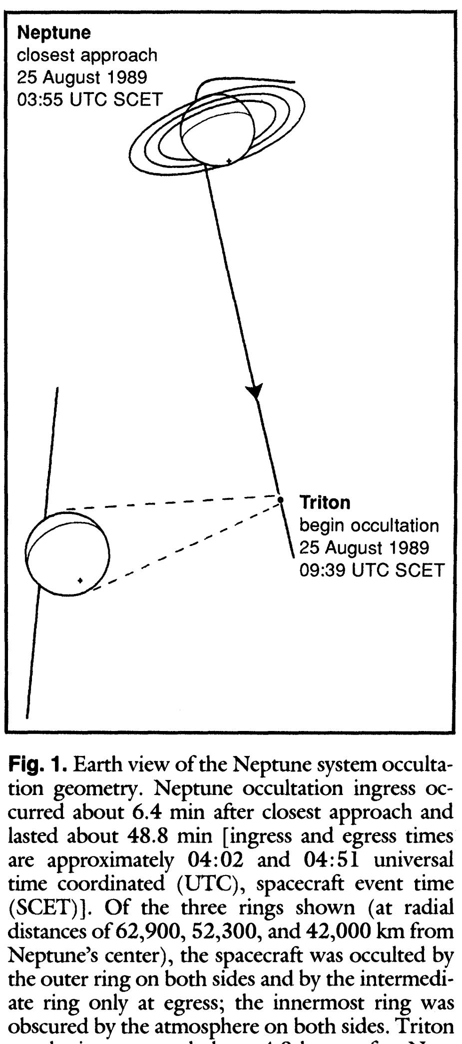

Fig. 1. Earth view of the Neptune system occultation geometry. Neptune occultation ingress occurred about 6.4 min after closest approach and lasted about 48.8 min [ingress and egress times are approximately 04:02 and 04:51 universal time coordinated (UTC), spacecraft event time (SCET)]. Of the three rings shown (at radial distances of 62,900, 52,300, and 42,000 km from Neptune's center), the spacecraft was occulted by the outer ring on both sides and by the intermediate ring only at egress; the innermost ring was obscured by the atmosphere on both sides. Triton occultation occurred about 4.8 hours after Neptune egress and lasted about 155 s (ingress and egress times approximately 09:39:29 and 09:42:04 UTC, SCET).

The next harmonic coefficient of interest for a planet in hydrostatic equilibrium is J_4. We find that this coefficient is much harder to determine than J_2 in the sense that it is far more sensitive to errors in modeling the nongravitational forces on Voyager 2, particularly forces generated on-board the spacecraft from the attitude control system and motions of the scan platform. Our best current estimate of J_4 depends on solutions for only J_2 and J_4 with all other harmonics set equal to zero, but with uncertainties of 2×10^{-6} accounted for in the harmonics J_3, J_5, and J_6. We recommend $J_4 = -26^{+12}_{-20}$ $(\times 10^{-6})$. Our estimate of the pole location referred to the B1950.0 equator and equinoxis α_{pole} (right ascension) $= 298.80 \pm 0.15°$ and δ_{pole} (declination) $= 42.86° \pm 0.10°$.

Neptune's atmosphere. The Voyager 2 observations included a radio occultation by Neptune with ingress at 61°N planetocentric latitude and egress at 44°S (Fig. 1). The initial results described below are based primarily on analysis of the "closed-loop" Doppler frequency data that are provided for monitoring purposes during the execution of the experiment (*5, 6*). At ingress, the Doppler data at 3.6 cm represent the occultation signals from a time well before any sensible occultation effects (16 min prior to closest approach) until the time when the angle of refraction of the signal propagating from the spacecraft through Neptune's atmosphere to Earth reached about 7°. For larger bending angles, the closed-loop data indicate an "out-of-lock" condition, due to the low signal strength, until the bending angle returned to about 6°. The data appear to be reliable from this point on through occultation egress. These closed-loop data extend to pressures of approximately 5×10^5 Pa (5 bars) at ingress and 4×10^5 Pa at egress.

One of the highest priority objectives of the Voyager 2 flyby was to determine the He abundance in the atmosphere of Neptune. When combined with similar measurements for Jupiter, Saturn, and Uranus, this measurement provides a fundamental constraint for theoretical models of the origin, evolution, and internal structure of the giant outer planets (*14, 15*). As in previous flybys of the Voyager mission, this is accomplished through intercomparison of measurements obtained with the infrared spectrometer and the radio occultation experiment. Although the reduction and assimilation of data is progressing, the results for the He abundance are not yet understood to our satisfaction. Until further progress is made in this area, we adopt the abundance ratio derived through application of this technique at Uranus (*15*) for use in reducing the occultation data.

Figure 2 shows atmospheric profiles derived through inversion of the 3.6-cm closed-loop data from both occultation ingress and egress (*16*). These initial results apply for an assumed He/H_2 abundance ratio of 15/85 by number, as discussed above, and for methane (CH_4) saturation below the tropopause; above the tropopause, the CH_4 mixing ratio is assumed to be about 3×10^{-5} by number as inferred from the vapor pressure at the tropopause (*17, 18*). For this composition, the temperature and pressure of the tropopause are near 50 K and 12×10^3 Pa, respectively, at ingress, and 49 K and 8×10^3 Pa at egress. Comparison of the two profiles in Fig. 2 reveals a vertically varying thermal contrast such that the stratosphere is warmer at ingress by as much as about 8 K near the 10^3-Pa pressure level, whereas the temperature in the troposphere is essentially the same at these two locations for pressures exceeding about 0.4×10^5 Pa. This result appears to be consistent with the meridional distribution of brightness temperatures inferred from latitude scans with the Voyager infrared spectrometer (*19*), which may be indicative of vertical variations in the zonal wind speed. In general, our temperature-pressure profiles compare favorably with the disk-averaged vertical structure derived from Earth-based observations of thermal emission from Neptune (*20*).

For pressures exceeding roughly 0.9×10^5 Pa, the observed temperature lapse rate in Fig. 2 corresponds closely to the adiabatic lapse rate computed when the specific heat of hydrogen is treated as a "frozen" equilibrium of the para-hydrogen and ortho-hydrogen states (*21*). The same situation is observed on Uranus (*12*) and provides an important constraint on the stability and convective dynamics of this region of the troposphere (*22*). However, this initial result should be interpreted with some caution because of the possible influence on the static stability of a vertically varying CH_4 abundance. In both profiles of Fig. 2, the maximum pressure is 1.2×10^5 Pa where the temperature is about 78 K. At greater pressures, the open-loop recordings contain the distinctive spectral signature of multipath propagation and a rapid decrease, followed by a recovery, in signal intensity of more than a factor of 10. We interpret these features as resulting from the presence of a cloud deck composed of CH_4, which is the likely condensate in this temperature range. As the closed-loop data system does not respond adequately to these types of signal behavior, reduction of the data to profiles at greater pressures cannot be completed until the open-loop data are fully reduced (*23*). However, one can establish a preliminary constraint on the CH_4 abundance below the condensation level by computing the saturation vapor pressure at the lowest level in the profile and comparing this with the total pressure. This procedure yields a lower limit on the CH_4 mixing ratio in the deep atmosphere of about 1% by volume, provided that our assumptions about the He abundance and the condition of CH_4 saturation below the tropopause are correct. This preliminary result is consistent with previous estimates from Earth-based observations (*24*) and represents an enhancement of C in the atmosphere of Neptune relative to a solar mixture by a factor of more than 10.

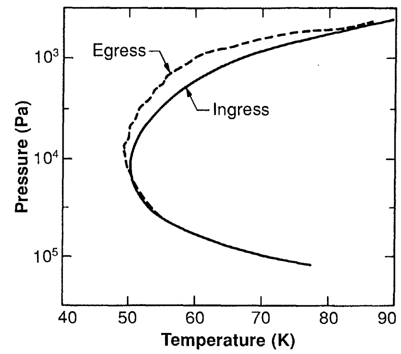

Fig. 2. Preliminary Neptune temperature-pressure profiles at planetocentric latitudes of 61°N (ingress) and 44°S (egress) from inversion of radio occultation data at 3.6 cm. The profiles correspond to an assumed He/H_2 mixing ratio of 15/85 by number density, and CH_4 saturation below the tropopause. Results will be extended to both lower and higher pressures when the complete data from the experiment are analyzed.

In the region beneath the CH_4 cloud, the 3.6-cm signal, and to a lesser extent the 13-cm signal, appears to have been absorbed by the atmosphere. As with the CH_4 cloud region, a more complete interpretation of the data at these pressures must await full analysis of the open-loop recordings. However, preliminary attempts to model the observations at pressures of several times 10^5 Pa suggest that ammonia (NH_3) at an abundance corresponding to its saturation vapor pressure may account for the apparent absorption. Other gases with appreciable vapor pressures at these temperatures (about 120 to 140 K), such as hydrogen sulfide (H_2S), do not appear to be capable of accounting for this observation, although only limited data are available on absorption under these atmospheric conditions. Our results to date are compatible with the NH_3 abundance of a few parts per million in the deep atmosphere inferred from Earth-based observations of the radio brightness of Neptune (*25*). If substantiated, the occultation-derived profile of NH_3 abundance would provide an important constraint on the composition of the lower atmosphere and cloud layers (*25, 26*). For example, an NH_3 vapor abundance as low as a few parts per million is sufficient under these atmospheric conditions to establish a strong upper bound on the abundance of H_2S vapor, unless the atmosphere is supersaturated with respect to the relatively involatile ammonium hydrosulfide solid.

The shape of a rapidly rotating, zonally symmetric fluid planet at pressure levels such as those discussed above is determined to a good approximation by a balance of gravitational, centrifugal, and Coriolis forces (*27*). We computed the size and shape of the 10^5-Pa isobaric surface in the southern hemisphere of Neptune using the results given above for the gravity field, the rotation period of the atmosphere as a function of latitude determined from Voyager imaging observations (*28*), and the radius at this pressure derived from the radio occultation measurements at egress. The equatorial and polar radii are 24,764 ± 20 and 24,340 ± 30 km, respectively, yielding an oblateness of 0.0171 ± 0.0015. At present, the major error source contributing to the uncertainties is the scatter in the observed atmospheric rotation periods. These values are compatible with analogous results for the 10^{-1}-Pa isobaric surface derived from Earth-based observations of stellar occultations by Neptune (*29*).

Neptune's ionosphere. The differential dispersive Doppler shifts observed with the closed-loop 3.6- and 13-cm receivers during ingress and egress show that Neptune has an extended ionosphere. Plasma is detected to an altitude of 5000 km above the 10^5-Pa pressure level. The topside scale height is about 1800 ± 300 km, corresponding to a plasma temperature of 950 ± 160 K if H^+ is the major ion. Figure 3 shows the topside of the ionosphere probed near the morning terminator during ingress at about 61°N. The density fluctuations above about 1600 km represent largely noise, but the local ionization peak at 1400 km represents a real layer. As in earlier studies of Jupiter, Saturn, and Uranus, the lower ionosphere appears to contain narrow layers of ionization, which produce multipath propagation during the occultation (*30*). Detailed study of this region also must wait until the primary data have been fully reduced.

Occultation by Triton. Geometrical characteristics of the occultation are given in Table 1 and Fig. 1, and our initial results are summarized in Table 1 and Figs. 4, 5, and 6. Detection and measurement of atmospheric and ionospheric effects were accomplished with both occultation ingress and egress data. These preliminary results are based on examination of the 3.6- and 13-cm open-loop data recorded at the Tidbinbilla tracking station.

Both the amplitude and phase of the 3.6- and 13-cm signals exhibit clear diffraction effects at occultation ingress and egress. Inverse Fresnel transform filtering procedures, developed for planetary ring studies (*31*), are used to correct for the diffraction (*32*). This treatment of the data is necessary because the small phase changes induced by the tenuous atmosphere are comparable with those induced by diffraction. As a measure of the success of the inverse Fresnel filtering, the reconstructed amplitude profiles exhibit transitions from full illumination to shadow over a processing resolution cell of 100 m in height, which is a small fraction of the natural Fresnel scales of about 1.0 and 1.9 km at 3.6- and 13-cm wavelength, respectively.

A by-product of the diffraction correction is a very accurate estimate of the time at which the spacecraft entered and exited Earth occultation. One may relate these times to radial distance from Triton's center by using the spacecraft trajectory. Our provisional radius for Triton based on the occultation geometry is 1355.4 ± 7 km (*10*). "Heights" discussed below are given relative to this provisional radius (*33*).

Diffraction-corrected signal phases are the primary data defining the atmosphere and ionosphere; signal amplitudes are not measurably affected by either. The two Voyager frequencies are coherently related by the ratio of 11 : 3, and we refer all results henceforth to the equivalent phase for the 3.6-cm wavelength signal. For analysis, rapidly changing phases of the received signals (up to about 5×10^{10} rad s^{-1}) are reduced to a near-zero rate by removing the effects of the trajectory, of predictable values of the reference oscillator frequency, and long linear trends to reduce remaining changes in phase of unknown origin. Any further change in phase (for example, of 1 rad at 3.6-cm wavelength) would correspond to: (i) an unmodeled change in distance between the spacecraft and the Earth tracking station (of 5.7 mm); (ii) a change in the columnar content of plasma electrons along the spacecraft-Earth path (of about 10^{16} m^{-2}); (iii) a change in the columnar content of neutral gas [of 5×10^{26} m^{-2} N_2 molecules along the path]; or (iv) an uncalibrated fractional change in the reference oscillator frequency (of about 2×10^{-11} for 1 s or of 2×10^{-12} for 10 s, and so forth).

Table 1. Occultation by Triton.

Geometrical characteristics
Radius = 1355 ± 7 km
Mass = 21.41 ± 0.07 ($\times 10^{21}$) kg
Density = 2054 ± 32 kg m^{-3}

Measure	Ingress	Egress
	Geometry	
Latitude (°)	+45	−16
Longitude (°)	+121	−143
Limb-spacecraft distance (km)	50.9×10^3	52.7×10^3
SZA* (°)	90.8	91.1
SZA 12 hours earlier (°)	91.6	70.2
	Ionosphere	
Height at peak (km)	350	340
Peak electron concentration (m^{-3})	23×10^9	46×10^9
Plasma scale height (km)		120
Topside plasma T for N_2^+ (K)		80
	N_2 atmosphere	
From the analytical model		
Surface p (Pa)	1.9	1.5
"Isothermal" T (K)	52	50
Surface concentration (m^{-3})	2.6×10^{21}	2.2×10^{21}
Equivalent vertical thickness (m-Am)	2.0	1.6
(indicated T at surface from fit to near-surface data, K)	(45)	(36)
Suggested representative values		
Surface p (Pa)	1.6 ± 0.3	
Equivalent isothermal T (K)	48 ± 5	
Surface T (K)	38	
CH_4 mixing ratio at surface	10^{-4}	

*Solar zenith angle.

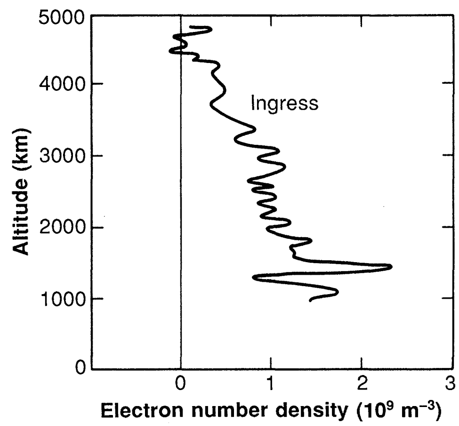

Fig. 3. Electron number density versus altitude above the 10^5-Pa (1 bar) pressure level on Neptune at 61°N. The profile is derived through inversion of radio occultation data at 3.6 and 13 cm. The overall slope of the curve is significant, as is the presence of the lowest few peaks shown. Below the lowest level shown, the data exhibit effects caused by narrow layers of ionization; however, the complete data set must be reduced before the profile can be extended through this region and before uncertainties in the curve shown can be evaluated.

Triton's ionosphere. Because of the coherent relationship between the signals, the two measured sequences of residual phase changes can be combined to cancel effectively any changes due to (i), (iii), and (iv), leaving (ii) as a self-calibrated or dispersive measure of the changes in plasma along the propagation path. This path includes Earth's ionosphere and the interplanetary medium, but the principal changes here are expected to be due to Triton's ionosphere because the ray path sweeps across it in about 2 min. Figure 4A shows the measured dispersive phase as a function of the height of ray periapsis, relative to an arbitrary zero value assumed in regions well above the ionosphere where this phase is not changing appreciably with altitude.

Figure 4B displays the ionospheric profiles of electron number densities as functions of height, obtained by Abel transform inversion (*16*) of the phase measurements, Fig. 4A. Peak number densities occur near 350-km altitude at the ingress location and at 340 km for egress. The peak value at ingress, $\sim 23 \times 10^9$ m^{-3}, is only half its value at egress, $\sim 46 \times 10^9$ m^{-3}. Deviations from zero of the number density recovered at low altitudes possibly result from violation of the assumption of spherical symmetry that is inherent in the Abel transform inversion or are an indication of changes along the remainder of the path. We interpret the $\pm 2.3 \times 10^9\ m^{-3}$ deviation as representative of the uncertainty in the peak estimates obtained. The abrupt change in the character of both profiles below ~200 km suggests that a sharp bottom to the ionosphere occurs at about this altitude.

The egress profile in particular appears similar to that of a classical single-layer ionosphere for which the measured topside plasma scale height can be used to define a plasma temperature provided that the principal ion can be identified. Several lines of evidence (*18, 34*) suggest that this is N_2^+ for Triton, for which the topside plasma temperature is about 80 ± 16 K. Of course, this would also be the temperature of the neutral species in this region if thermal equilibrium has been established with the ions. The ingress ionosphere appears less well developed, with markedly lower density and a less regular topside shape. The difference in number densities may be due to the fact that, although grazing solar illumination is about the same at both locations at the time of the measurement, the egress location received more direct sunlight previously, as evidenced in Table 1 by the location of occultation points and the nature of their changing solar zenith angles. In fact, the sun was below the horizon at the ingress surface location for the total Triton day but it was above for 61% of the day at egress. Precipitating particles from Neptune's magnetosphere might also be differentially affecting the two ionospheric regions.

Triton's atmosphere. Measured phase as a function of time or height above Triton's surface for the 3.6-cm signal can be corrected for plasma effects from the dispersive measure of (ii), discussed above, leaving a combined measure of the (i), (iii), and (iv) effects described previously. We want to determine (iii). The ray paths sweep over the height range of the sensible neutral atmosphere in about 10 s, and (i) is not a problem on this time scale. However, random changes in the reference oscillator frequency (iv) occur on all time scales. In order to characterize the total error, we spline-fitted the dispersion-corrected and diffraction-corrected phase and subtracted the trends to remove variations on time scales greater than 10 s. The zero-mean resulting phase above the atmosphere has root-mean-square (rms) deviations of about 0.16 rad and peak values of up to nearly 0.5 rad. The total phase shift at the surface as compared with the trend is about 2 rad. Thus, we conclude that we can obtain reasonably good values for the surface pressure and an equivalent isothermal temperature for the atmosphere at occultation ingress and egress. Our estimates of error remain, necessarily at this point, somewhat subjective.

We proceed by fitting analytical "lightcurves" to the data, using methods similar to the methods for analysis of stellar occultations, but in this case we use the measured phase retardation along the occultation ray rather than intensity as the observable. It is assumed that the refraction is due to N_2 (*18, 34*). We have objectively searched for a four-parameter best fit (in a least-squares sense) of analytical representations of the atmosphere to the diffraction-corrected phase for the heights from 120 km to the surface at both occultation locations (*35*). We did not conduct an exhaustive search of the error surface for all possible localized minima but did find distinct results for both ingress and egress. The four parameters found in this

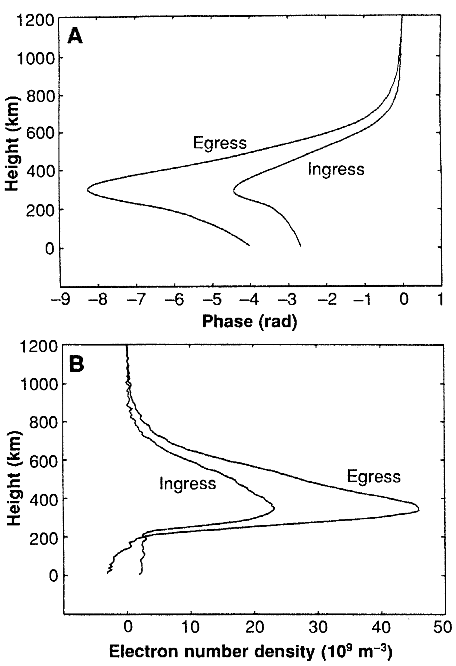

Fig. 4. (**A**) Observed 3.6 cm–wavelength phase variation of occultation radio signal in Triton's ionosphere. The ionosphere signature extends to nearly 1000 km above the surface in both cases. (**B**) Electron number density profiles obtained from inversion of the observed phase profiles in (A). The peak electron densities are reached at about the same height (~340 to 350 km), but the egress peak value is nearly twice the ingress value. The marked difference between ingress and egress may be due to different solar illumination conditions. A sharp bottom to the ionosphere appears to be reached at an altitude of about 200 km.

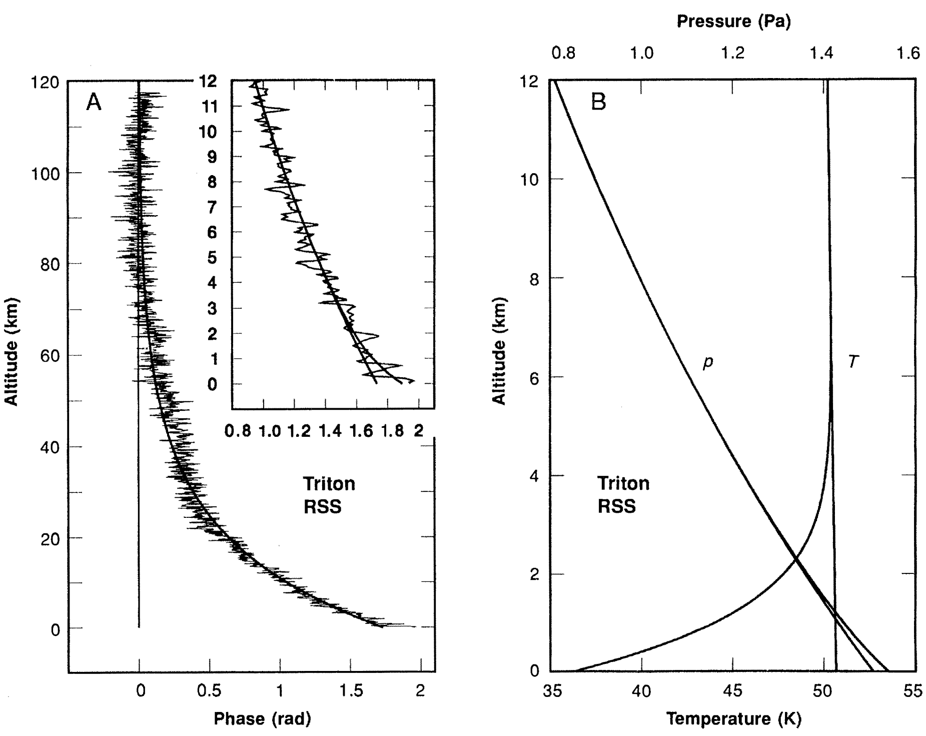

Fig. 5. (**A**) Phase measurements at 3.6 cm–wavelength near Triton's limb at egress after diffraction and plasma effects have been removed. The smooth curve embedded in the data is the result of a least-squares fit of a four-parameter function, which includes an analytical "isothermal" atmosphere and a linear term for the oscillator drift, shown here as the vertical line [see text, (*35*)]. The expanded scale in the inset shows an improved fit to the data with a curve pulling (or branching) to the right in lower atmosphere, as obtained by use of two additional parameters in the fitting function (*35*). (**B**) Temperature and pressure profiles resulting from the fits to the phase depicted in (A), on the assumption that the atmosphere consists entirely of N_2. The isothermal fit produces the right temperature profile and left pressure profile; the analytical representation of a thermal inversion in the atmosphere gives the left temperature profile and the right pressure profile.

way represent both a reference phase baseline and an "isothermal" atmosphere (*35*). The egress results are shown in Fig. 5A (*36*). The fit has an rms error relative to the data of 0.07 rad. This profile corresponds to a surface pressure of 1.5 Pa (15 μbar) and an equivalent isothermal temperature of 50 K. For ingress, the corresponding numbers are 0.08-rad rms error, 1.9 Pa, and 52 K. At the present level of understanding, the differences between ingress and egress are not considered significant. In considering the overall problem, we suggest preliminary single representations for surface pressure and equivalent isothermal temperature of 1.6 ± 0.3 Pa (16 ± 3 μbar) and 48 ± 5 K, respectively.

It could be that Triton's atmosphere is controlled by vapor-pressure equilibrium (VPE) with surface ices of N_2 and CH_4, even though vapor pressures at 48 ± 5 K are at least 25 Pa for N_2 and 0.006 Pa for CH_4 (*37*). The occultation locations could be ice-free, with the control being exerted only over limited colder regions.

It is also possible that the occultation points have much colder near-surface atmospheres and surfaces than the equivalent isothermal atmospheric temperature. To investigate this, we add two more free parameters, keeping fixed the four found above in the isothermal fit (*35*). The two new parameters are chosen so as to allow a departure to either warmer or colder temperatures in the lower part of the atmosphere, to the extent that this would further reduce the rms error of the overall fit relative to the data. The residual is in fact reduced slightly at both locations by solutions that correspond to the addition of a thermal inversion within about 5 km of the surface. Such an inversion is akin to those observed over the carbon dioxide (CO_2) polar caps of Mars (*38*) and proposed to explain stellar occultation results for Pluto (*39, 40*). The inset in Fig. 5A shows the improved fit to the lower atmospheric egress data obtained with the inversion, and Fig. 5B displays the temperature and pressure profiles for this region for both the isothermal and thermal inversion models. Table 1 gives the surface temperatures corresponding to the inversion case, where the specific values are of less significance than the fact that they are markedly below those given by the isothermal fits alone and could correspond to VPE with surface ices.

Our understanding of the reference oscillator stability is such that we cannot assert now, from our data, that there is a near-surface temperature inversion at the occultation points. Our purpose is to demonstrate that the data do not exclude this possibility and that they provide some reason to include it. Results of the Voyager infrared interferometry investigation are supportive of this interpretation because they indicate a temperature for the surface of 39^{+3}_{-4} K (*19*). For VPE of N_2 and CH_4 at a total pressure of 1.6 Pa, the temperature of the atmosphere at the surface would be 38 K and the CH_4/N_2 mixing ratio would be about 10^{-4}.

Extended limb hazes are seen in the Triton images (*28*). The derived pressures and equivalent isothermal temperatures appear to rule out VPE with suspended N_2 and CH_4 ice (or liquid) particles in the measured atmosphere, unless there is a sharp dip in temperature in the higher regions. If the mixing ratio is set by VPE at the surface, then an ice crystal haze formed at such a temperature minimum might be composed mostly of CH_4 particles. Localized N_2 condensate clouds may be formed by venting from the surface (*28*). There are, of course, other possibilities for aerosol formation and atmospheric haze distinct from the direct condensation of CH_4 and N_2 (*41*).

From the radio occultation measurements of pressure and temperature in the troposphere and of temperature in the ionosphere, plus the radio measures of Triton's radius and mass, one can make a rough approximation to the T-$p(h)$ structure [temperature-pressure (as a function of height)] of Triton's atmosphere to great height, as shown in Fig. 6. It is assumed that the ionospheric plasma temperature of 80 K applies also to the neutral N_2 over the ionospheric height range of 200 to 800 km and that the lower atmospheric measurements apply from the surface to a height of 50 km. If we use the derived surface pressure of 1.6 Pa and an equivalent isothermal temperature of 48 K and linearly interpolate the temperature between 50 and 200 km, we find a pressure of 2.0×10^{-7} Pa (2.0 pbar) at 600 km, for example. This is at the middle of the altitude range where the ultraviolet spectroscopy (UVS) experiment measured the N_2 concentration. From the radio experiment the corresponding N_2 number density is 1.8×10^{14} m^{-3}, which is about 25% below the density at 600 km as derived from the UVS observation (*18*). This near agreement is surprisingly good, in view of the large extrapolation and the various uncertainties in both experimental areas, as well as the differing locations of the measurements at Triton.

Conclusions. Although analysis of the RSS data is in a preliminary state, our initial results show Neptune and its companion Triton to be distinct from any other planet and satellite in our solar system: Neptune, although farthest from the sun, has a well-developed ionosphere; the atmospheric composition is both distinctive and complex. Triton has a tenuous atmosphere and a

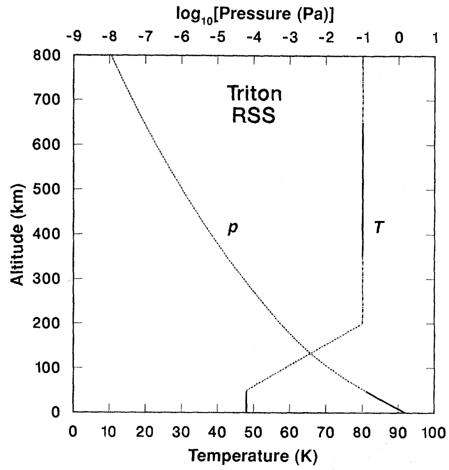

Fig. 6. Large-scale T-$p(h)$ profile constructed on the basis of the use of the equivalent isothermal temperature of 48 K from 0 to 50 km, the ionospheric plasma temperature of 80 K from the bottom of the detectable ionosphere at an altitude of 200 km to 800 km, near the top of the detectable ionosphere, with linear interpolation between 50 and 200 km. The pressure profile is derived from constructed temperature profile and the 1.6-Pa surface pressure. The N_2 number density obtained by this procedure at 600 km is 1.8×10^{14} m^{-3}, which is about 25% less than the density reported from the UVS observation (*18*) at 600 km.

substantial ionosphere contained in a single, near classical layer; our results for the atmospheric structure include the suggestion of a strong temperature inversion within about 5 km of the surface. Refinement and extension of these results can be expected as the reduction and analysis of the primary data set proceed.

REFERENCES AND NOTES

1. V. R. Eshleman *et al.*, *Space Sci. Rev.* **21**, 207 (1977); V. R. Eshleman *et al.*, *Science* **204**, 976 (1979); V. R. Eshleman *et al.*, *ibid.* **206**, 959 (1979); G. L. Tyler *et al.*, *ibid.* **212**, 201 (1981); G. L. Tyler *et al.*, *ibid.* **215**, 553 (1982); G. L. Tyler *et al.*, *ibid.* **233**, 79 (1986).
2. G. L. Tyler, *Proc. IEEE* **75**, 1404 (1987).
3. R. E. Edelson *et al.*, *Science* **204**, 913 (1979).
4. Signal-to-noise ratios (SNR) of approximately 36,000 and 890 were achieved at 3.6 and 13 cm, respectively, from the Deep Space Network 70-m antenna with 1-s integration intervals. Future combining of the 3.6-cm signals from Tidbinbilla and Parkes and the 13-cm signals from Tidbinbilla and Usuda should increase the effective SNR by roughly 60% at both wavelengths.
5. Real-time monitoring data include, in part, measurements of signal amplitude, Doppler frequency, and the frequency dispersion between the 3.6- and 13-cm signals at time resolutions of about 1 s.
6. Primary data for the radio occultation measurements consist of sample measurements of the antenna terminal voltages recorded on computer-compatible tape at rates between 50,000 and 80,000 samples per second, depending on the receiving site. These data are referred to as "open-loop" data, as they are collected without the aid of signal tracking. A second data set, also of high quality, obtained only from the Tidbinbilla station, comprises Doppler frequency measurements at each wavelength plus a measure of the signal amplitude. This set of data is

referred to as "closed-loop" data, as it is obtained from automatic tracking receivers operating on the principle of the phase-locked loop; the term "closed-loop" refers to the feedback control aspects of the system. As the closed-loop receivers cannot track signals with dynamic characteristics that exceed limited thresholds (for a given SNR) and can track only a single frequency mode, they are not useful in obtaining data from regions that produce multipath propagation or rapidly varying amplitude. For occultation measurements the spacecraft signal is derived from a highly stable on-board reference oscillator (*2*). Gravity observations are obtained with closed-loop data from the ground system, but in this case the spacecraft transmitter frequency is derived from an uplink signal radiated earlier from the ground. Over long time periods this system achieves essentially the stability of the station atomic clocks, which are H_2 maser frequency standards. In this round-trip, uplink-downlink mode, the observations are referred to as "tracking data."

7. Preliminary 3.6 cm–wavelength diffraction-corrected occultation data do not reveal Neptune's rings. As discussed in the caption to Fig. 1, the geometric opportunity for the detection of rings is limited and most promising for occultation egress. Radial locations of the known rings were probed during the time that Voyager 2 was also behind the ionosphere of Neptune, for both occultation ingress and egress. The diffraction correction thus is made more complex in that the rapidly changing ionospheric component of the signal phase must be removed from the data. Our preliminary procedures are heuristic. It may be possible to improve on the present result in the future. Our calculations of the ring geometry show the major condensations of material, as seen in Voyager images of the outermost ring at 62,900 km, to be located about 60° and 95° in orbital phase from the position of the radio occultation cuts for ingress and egress, respectively.
8. In units of the ratio of the mass of the sun to the mass of the Neptune system, S. Newcombe [*Astron. Pap. Am. Ephemeris* 7 (1898)] determined a value of 19,314 based on observations of Uranus (1781 to 1896) and Triton. Later, P. K. Seidelmann, R. L. Duncombe, and W. J. Klepczynski [*Astron. J.* **74**, 776 (1969)] obtained a value of 19,349 ± 31 with observations of Uranus (1781 to 1968), and M. E. Ash, I. I. Shapiro, and W. B. Smith [*Science* **174**, 551 (1971)] obtained a value of 19,400 ± 100 from a database including optical observations of the sun and planets from 1750 to 1970. Several determinations derived from the observed orbital period and orbital radius of Triton and Nereid have been reviewed by F. Mignard [*Astron. J.* **86**, 1728 (1982)] and by V. Veillet [*Astron. Astrophys.* **112**, 277 (1982)]. Because of the difficulty of ground-based satellite astrometry at the distance of Neptune, the satellite technique yielded little or no improvement in accuracy.
9. In deriving the ratio of the mass of the sun to that of a planet, a value of $GM_{sun} = 1.327124408 \times 10^{11}$ $km^3\ s^{-2}$ is used. It is the best determined constant in astronomy and is accurate to the number of digits given. It is determined from accurately known periods of the planets together with distance measurements between Earth and Mars by means of radio ranging to the Viking Landers between 1976 and 1982; see R. D. Reasenberg *et al.*, *Astrophys. J.* **234**, L219 (1979); *The Astronomical Almanac for the Year 1988* (Government Printing Office, Washington, DC, 1987); A. M. Nobili and C. M. Will, *Nature* **320**, 39 (1986).
10. This value for the radius is from the radio occultation event times and the most recent solution for the spacecraft trajectory, on the assumption that Triton is spherical. For consistency between ingress and egress, this method required a shift of the spacecraft position by ~10 km along the trajectory in the plane of the sky. The error bars assume a remaining cross-track uncertainty of 12 km, which is comparable to that achieved for Uranus but which is also much less than the quoted formal errors at this time. From the geometry, the radius error is then about 60% of this value. Until final, realistic uncertainties are obtained, this reliability is provisional.
11. W. B. McKinnon and S. Mueller [*Geophys. Res. Lett.* **16**, 591 (1989)] have computed models of differentiated ice-rock satellites as a function of radius. From our density of 2054 kg m^{-3}, their results imply a mass fraction of 0.70 anhydrous rock for Triton. According to these models, both Triton and Pluto are so rock-rich that it may be difficult to explain their formation in terms of direct condensation from the primordial solar nebula. A. J. R. Prentice (personal communication) avoids this problem with a lower mass fraction of rock (48%), but his models require controversially large mass fractions of CO_2 ice (19%), clathrated CH_4 (29%), and graphite (4%).
12. G. F. Lindal *et al.*, *J. Geophys. Res.* **92**, 14987 (1987).
13. R. A. Jacobson, personal communication.
14. J. B. Pollack *et al.*, *Icarus* **67**, 409 (1986); J. B. Pollack and P. Bodenheimer, in *Origin and Evolution of Planetary and Satellite Atmospheres*, S. K. Atreya, J. B. Pollack, M. S. Matthews, Eds. (Univ. of Arizona Press, Tucson, 1989), pp. 564–602.
15. B. J. Conrath *et al.*, *J. Geophys. Res.* **92**, 15003 (1987).
16. G. Fjeldbo *et al.* [*Astron. J.* **76**, 123, Appendices A, B, and C (1971)] describe the fundamental problem for spherical planets and give both numerical and exact Abel transform solutions for inversion; G. F. Lindal *et al.* [*Astron. J.* **90** (no. 6), 1136, Appendix (1985)] extend the procedure to oblate planets described by shells in local hydrostatic equilibrium; G. F. Lindal *et al.* [*J. Geophys. Res.* **92** (no. A13), 14987, Appendix (1987)] elaborate on the interpretation of refractivity profiles in terms of density, pressure, and temperature when nonuniformly mixed gases are considered.
17. G. S. Orton *et al.* [*Icarus* **70**, 1 (1987)] inferred a stratospheric CH_4 mixing ratio of 0.02 from Earth-based observations of Neptune near 8 μm. However, it is difficult at present to understand how such a large amount of CH_4 can be maintained in the stratosphere. Until this result is substantiated, we adopt the more conservative value, 3×10^{-5}, for the CH_4 abundance in the stratosphere, an assumption that is consistent with initial results reported by A. L. Broadfoot *et al.* (*18*) on the basis of observations of Neptune with the Voyager ultraviolet spectrometer.
18. A. L. Broadfoot *et al.*, *Science* **246**, 1459 (1989).
19. B. J. Conrath *et al.*, *ibid.* 1454 p.
20. J. F. Appleby, *Icarus* **65**, 383 (1986).
21. For discussion of the specific heat of hydrogen, see L. M. Trafton, *Astrophys. J.* **147**, 765 (1967) and L. Wallace, *Icarus* **43**, 231 (1980).
22. P. J. Gierasch and B. J. Conrath, *J. Geophys. Res.* **92**, 15019 (1987).
23. Multipath propagation generally results from a local change in the vertical gradient of the refractive index. Such effects occur in association with sharp temperature changes, and in clouds. Here, we find a CH_4 cloud likely on the basis of current ideas about the structure of the Neptune atmosphere (*20, 24*) and by analogy with the Voyager radio occultation study of the atmosphere of Uranus (*12*). The inversion performed for this report to find the refractivity profile is based on "closed-loop" data (*6*), which are limited to tracking a single propagation mode. Preliminary examination of the "open-loop" data from Tidbinbilla show the simultaneous presence of multiple signals at different frequencies.
24. G. S. Orton *et al.*, *Icarus* **67**, 289 (1986); J. T. Bergstralh and K. H. Baines, in *Uranus and Neptune*, J. T. Bergstralh, Ed. (Conference Publication 2330, NASA, Washington, DC, 1984), p. 179; G. S. Orton and J. F. Appleby, *ibid.*, p. 89.
25. P. N. Romani *et al.*, *Geophys. Res. Lett.* **16**, 933 (1989).
26. J. S. Lewis, *Icarus* **10**, 365 (1969).
27. G. F. Lindal *et al.*, *Astron. J.* **90**, 1136 (1985).
28. B. A. Smith *et al.*, *Science* **246**, 1422 (1989).
29. The most complete and accurate stellar occultation results on the radius and oblateness of Neptune are reported by W. B. Hubbard *et al.* [*Icarus* **72**, 635 (1987)] and R. G. French *et al.* [*Astron. J.* **90**, 2624 (1985)]. Before making this comparison, we reinterpreted the results reported in these references to take account of recent improvements in determinations of the orientation of Neptune's spin axis, such as was derived from our investigation of Neptune's gravity field (see text). Results for the two isobaric surfaces, 10^{-1} and 10^5 Pa, then appear to be compatible both in absolute radius and in oblateness when a reasonable model is adopted for the intervening thermal structure.
30. For results from Jupiter, see G. Fjeldbo *et al.* [*Astron. Astrophys.* **39**, 91 (1975)] and G. Fjeldbo *et al.* [in *Jupiter*, T. Gehrels, Ed. (Univ. of Arizona Press, Tucson, 1976), pp. 238–246]; for results from Saturn, see G. F. Lindal *et al.* [*Astron. J.* **90**, 1136 (1985)]; for results from Uranus, see (*12*).
31. For a survey and guide to the literature, see (*2*); E. A. Marouf *et al.* [*Icarus* **66**, 120 (1986)] give the theoretical basis.
32. Here we treat the atmosphere of Triton as a "thin screen" and refer our results to the plane containing the instantaneous limb of Triton. Observations at 3.6 and 13 cm are individually inverse Fresnel–transformed relative to this plane. All interpretation of the atmosphere is then carried out on the two diffraction-corrected data sets. From the results, the maximum bending angle of the refracted rays grazing the surface of Triton is about 10^{-6} rad, so the thin-screen approximation appears to be valid.
33. The geometry is such that an error ΔR in the radius R_0 of Triton causes error Δh in the height h: $\Delta h \approx -h\Delta R/(R_0 + h)$. We anticipate small adjustments to the height scale, on the order of 1 to 10 km, when the final trajectory reconstruction becomes available.
34. S. K. Atreya, in a paper presented at the spring meeting of the American Geophysical Union, Baltimore, May 1989, predicted the presence of an ionosphere with peak electron concentrations in the range of $20 \times 10^9\ m^{-3}$ at an atmospheric density of N_2 in the range 10^{16} to $10^{17}\ m^{-3}$.
35. The model we use for the phase observable is

$$\phi = A_0 + A_1 \frac{R - R_0}{R_0} + P_1 \left(\frac{R_0}{R}\right)^{q1} + P_2 \left(\frac{R_0}{R}\right)^{q2}$$

where R_0 is the Triton radius. For the "isothermal" atmosphere only the first three terms on the right side with the four parameters A_0, A_1, P_1, q_1 are used; this actually corresponds to temperature being inversely proportional to radius, but the result is essentially a constant over the small radial extent of the sensible neutral atmosphere. For the "inversion" atmosphere, the last term with parameters P_2, q_2 is added, while the first four parameters are held at the isothermal values. Eshleman (*39*) described essentially this model in more detail in a study of stellar occultation data from Pluto. The data used are diffraction-corrected to 100-m radial resolution. In our application, stable results are obtained from use of the first three terms, where the A_0, A_1 terms describe the baseline phase and linear phase drift while P_1 and q_1 set the atmospheric surface density and scale height. Addition of the fourth term reduces the rms error further. In solving for P_2, q_2, the search for best fit is begun with initial values corresponding to small scale height in order to select the minimum solution associated with the trends in data near Triton's surface (see Fig. 5A); other minima in the rms residuals for the six-parameter model can be found, but they correspond to fitting of the large fluctuations above an altitude of about 30 km. We obtain for the Triton occultation egress (Fig. 5) $A_0 = 30.9$, $A_1 = -0.103$, $P_1 = 1.73$, $q_1 = 68.2$, $P_2 = 0.163$, $q_2 = 1379$, where the A and P values are in radians; for Triton occultation ingress, not shown, $A_0 = 8.40$, $A_1 = 0.399$, $P_1 = 2.12$, $q_1 = 65.1$, $P_2 = 0.0832$, $q_2 = 1393$. The A_0, A_1 obtained by these fits represent linear trends in the phase that agree with the observed phase at an altitude of about 120 km, where there is no mixing of oscillator and atmospheric effects. Additional work on this analysis is needed to establish the errors objectively.
36. Figure 5A shows obvious deviations of the data from the best fit model curve, especially in the height range of roughly 20 to 60 km; some of these deviations are as large as or larger than the increase in phase within the lowest few kilometers of the atmosphere corresponding to a possible thermal inversion (*35*). At the present stage of analysis, we are unable to distinguish between the primary alternatives of thermal structure in the atmosphere and oscillator noise as the source of these deviations. With regard to the deviation near the surface, very

similar structure is observed at both occultation points [see model constants in (35)]. With regard to the region between 20 and 60 km, the deviations from the model curves are similar at both occultation points. Astute readers can infer the type of thermal structure required to explain these deviations by comparison with the reference model curves shown.
37. G. N. Brown and W. T. Ziegler [in *Advances in Cryogenic Engineering*, Vol. 25, K. D. Timmerhaus and H. A. Snyder, Eds. (Plenum, New York, 1979), p. 662] give polynomial fits to vapor pressure data.
38. G. F. Lindal *et al.*, *J. Geophys. Res.* **84**, 9443 (1979).
39. V. R. Eshleman, *Icarus* **80**, 439 (1989).
40. W. B. Hubbard *et al.*, *ibid.*, in press.
41. W. R. Thompson *et al.*, *Geophys. Res. Lett.* **16**, 981 (1989).
42. This experiment required extensive support from NASA headquarters and, at the Jet Propulsion Laboratory (JPL), from the Voyager Project, the Office of Tracking and Data Acquisition, and the Deep Space Network. Members of the Radio Science Support Team at JPL charged with the implementation and execution of the experiment included A. Densmore, M. Delitsky, P. Eshe, and Y. H. Son, and we thank them and their colleagues for major, sustained efforts in carrying out this experiment; two other members of this team, S. Asmar and D. Morabito, deserve special credit for their critical roles in the encounter preparation and real-time operations. Voyager Project Management contributed to a highly enhanced scientific return by agreeing to and supporting an extremely challenging encounter scenario. The personnel of the Deep Space Communication Complex at Tidbinbilla and at the CSIRO Parkes Radio Astronomy Observatory (RAO) in Australia deserve special mention; their participation and efforts to improve radiometric performance far exceeded the demands of their normal duties. For the first time, we were joined by colleagues from the Japanese Institute of Space and Astronautical Science, who provided the facilities of the Usuda Deep Space Station and who were responsible for the development and execution of the observations in Japan. We are pleased with the technical exchange and relationships this collaboration brought about. The Radio Science experiments could not have succeeded without the ability to use navigation data taken within about 30 hours of closest approach to fine-tune the spacecraft events for the exacting geometry of a flyby only 4900 km above the cloud tops of Neptune. A 16-s error in estimated arrival time would have resulted in a complete loss of the primary occultation data (and the error was this large 2 days before closest approach); as it developed, the actual arrival time was within 1 s of the last arrival time prediction. The Voyager Navigation Team accomplished this extraordinary feat. F. Donivan, of the S. S. Freedom Office, NASA, performed a real-time liaison function between JPL and Parkes RAO. At Stanford, M. Maurer and T. Spilker contributed importantly to pre-encounter analyses and preparation, encounter operations, and data reduction; H. Rand provided much support, coordination, and help in the preparation of the experiment and of this manuscript.

31 October 1989; accepted 15 November 1989

Magnetic Fields at Neptune

NORMAN F. NESS, MARIO H. ACUÑA, LEONARD F. BURLAGA, JOHN E. P. CONNERNEY, RONALD P. LEPPING, FRITZ M. NEUBAUER

The National Aeronautics and Space Administration Goddard Space Flight Center–University of Delaware Bartol Research Institute magnetic field experiment on the Voyager 2 spacecraft discovered a strong and complex intrinsic magnetic field of Neptune and an associated magnetosphere and magnetic tail. The detached bow shock wave in the supersonic solar wind flow was detected upstream at 34.9 Neptune radii (R_N), and the magnetopause boundary was tentatively identified at 26.5 R_N near the planet-sun line (1 R_N = 24,765 kilometers). A maximum magnetic field of nearly 10,000 nanoteslas (1 nanotesla = 10^{-5} gauss) was observed near closest approach, at a distance of 1.18 R_N. The planetary magnetic field between 4 and 15 R_N can be well represented by an offset tilted magnetic dipole (OTD), displaced from the center of Neptune by the surprisingly large amount of 0.55 R_N and inclined by 47° with respect to the rotation axis. The OTD dipole moment is 0.133 gauss-R_N^3. Within 4 R_N, the magnetic field representation must include localized sources or higher order magnetic multipoles, or both, which are not yet well determined. The obliquity of Neptune and the phase of its rotation at encounter combined serendipitously so that the spacecraft entered the magnetosphere at a time when the polar cusp region was directed almost precisely sunward. As the spacecraft exited the magnetosphere, the magnetic tail appeared to be monopolar, and no crossings of an imbedded magnetic field reversal or plasma neutral sheet were observed. The auroral zones are most likely located far from the rotation poles and may have a complicated geometry. The rings and all the known moons of Neptune are imbedded deep inside the magnetosphere, except for Nereid, which is outside when sunward of the planet. The radiation belts will have a complex structure owing to the absorption of energetic particles by the moons and rings of Neptune and losses associated with the significant changes in the diurnally varying magnetosphere configuration. In an astrophysical context, the magnetic field of Neptune, like that of Uranus, may be described as that of an "oblique" rotator.

NEPTUNE HAS BEEN DISCOVERED to have an intrinsic planetary magnetic field B and magnetosphere on the basis of data obtained during the close approach by Voyager 2 (V2) on 25 August 1989. The instrumentation (*1*) for magnetic field measurements on Neptune, which had been used to make observations of the magnetic fields of Jupiter (*2*), Saturn (*3*), and Uranus (*4*), operated normally throughout the entire encounter. The dual low-field magnetometers (LFMs) may automatically change ranges every 4.8 s, as required by the magnitudes of the measured magnetic field components. The minimum quantization uncertainty is ±0.002 nT in the lowest range (±8 nT full scale) and increases to ±12.2 nT in the highest range of ±50,000 nT, used near closest approach (CA). The twin high-field magnetometers (HFMs) also provided data during this encounter (the large fields measured near CA were well within their lower range of ±50,000 nT, with a quantization uncertainty of ±12.2 nT). Vector measurements for the LFMs were obtained at intervals of 60 ms and were subsequently averaged over 1.92 s, 9.6 s, 48 s, 8 min, and 1 hour for this study. The HFM measurements were made at 0.6-s intervals and are primarily used within 2 R_N of the planet, where the field is larger than 2000 nT.

The spacecraft trajectory during flyby and the obliquity of Neptune led to a sequence of observing positions within the magnetosphere that ranged from 26°S while inbound, increasing up to a maximum northerly latitude of 79°N near CA, and then decreasing to 21°S outbound. The spacecraft was within the magnetosphere and magnetotail of the planet for approximately 38 hours. There were no close encounters with any Neptunian moon, as by Voyager 1 at Titan (*5*), although the trajectory had been chosen so that it passed to within 38,000 km of Triton. Before the V2 encounter, very little was known about the possible existence and characteristics of any Neptunian magnetic field and radiation belts because indisputable identification of nonthermal radio emissions was lacking (*6*). A number of predictions of the magnetic field at Neptune had been made before encounter (*7*), covering a range of values from 0.3 to 17 G.

This preliminary report is based on data

N. F. Ness, Bartol Research Institute, University of Delaware, Newark, DE 19716.
M. H. Acuña, L. F. Burlaga, J. E. P. Connerney, R. P. Lepping, Laboratory for Extraterrestrial Physics, NASA Goddard Space Flight Center, Greenbelt, MD 20771.
F. M. Neubauer, Institut für Geophysik und Meteorologie, Universität zu Koln, D-5000 Koln 41, Federal Republic of Germany.